Biophysical Journal, Volume *111*

Supplemental Information

Spindle Size Scaling Contributes to Robust Silencing of Mitotic Spindle Assembly Checkpoint

Jing Chen and Jian Liu

Supplementary Materials

Spindle size scaling contributes to robust silencing of mitotic spindle assembly checkpoint

J. Chen, J. Liu

Supplementary figures

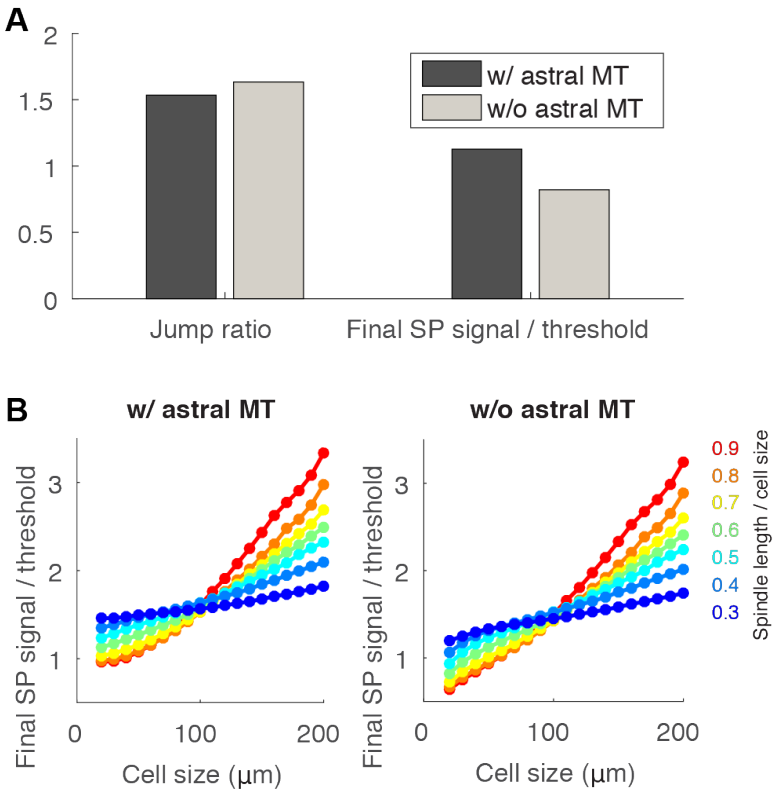

Figure S1: **Astral microtubules do not affect results significantly.** (**A**) Comparison between cases with and without astral microtubules under default geometric settings. (**B**) Results with different cell size and spindle size. Left panel is identical to Figure 4B in main text. Right panel results from simulations without astral microtubules.

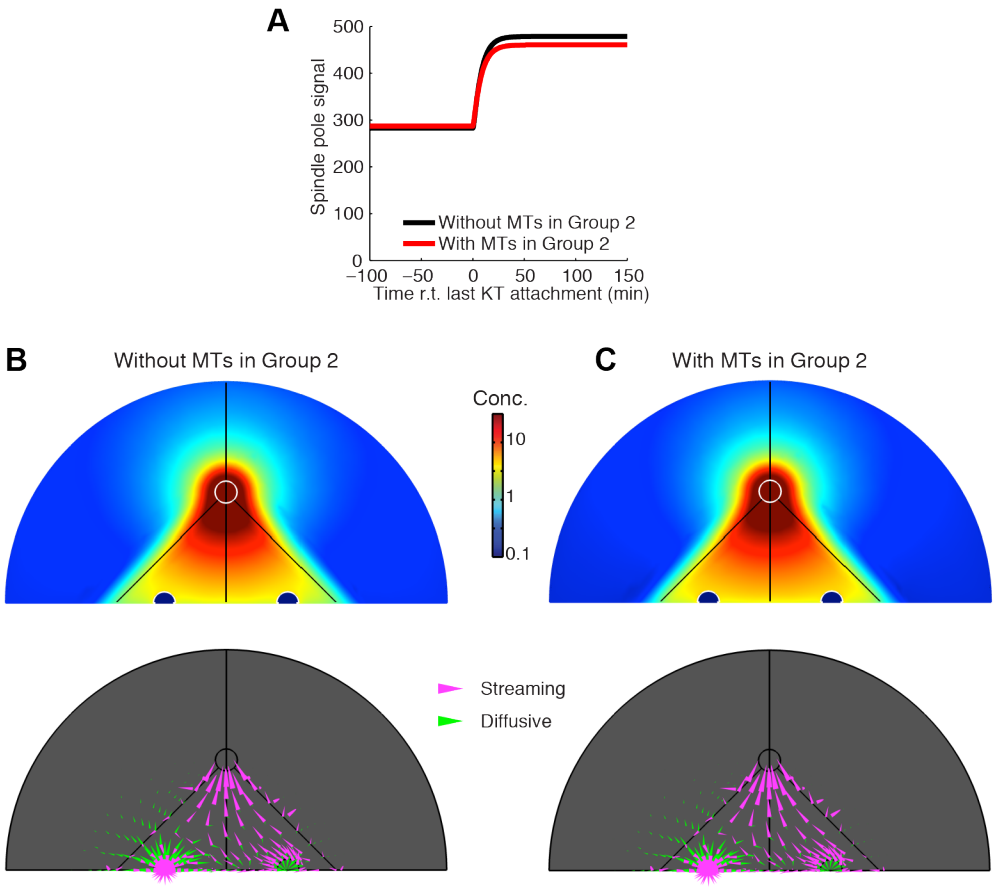

Figure S2: **Comparison between original model and improved model.** (**A**) Comparison of results from the original model (without microtubules in Group 2) and improved model (with microtubules in Group 2). The improved model does not change the step change in the spindle pole signal after the last kinetochore attachment. Results with default geometric setup: Δ = 20μm, $L = W$ = 10μm, δ = 1μm. (**B**) and (**C**) Detailed results from the original model and improved model. Upper panels: final steady state concentration gradient of SAC proteins. Lower panels: Fluxes of SAC proteins in the streaming or diffusive states before the last kinetochore attachment.

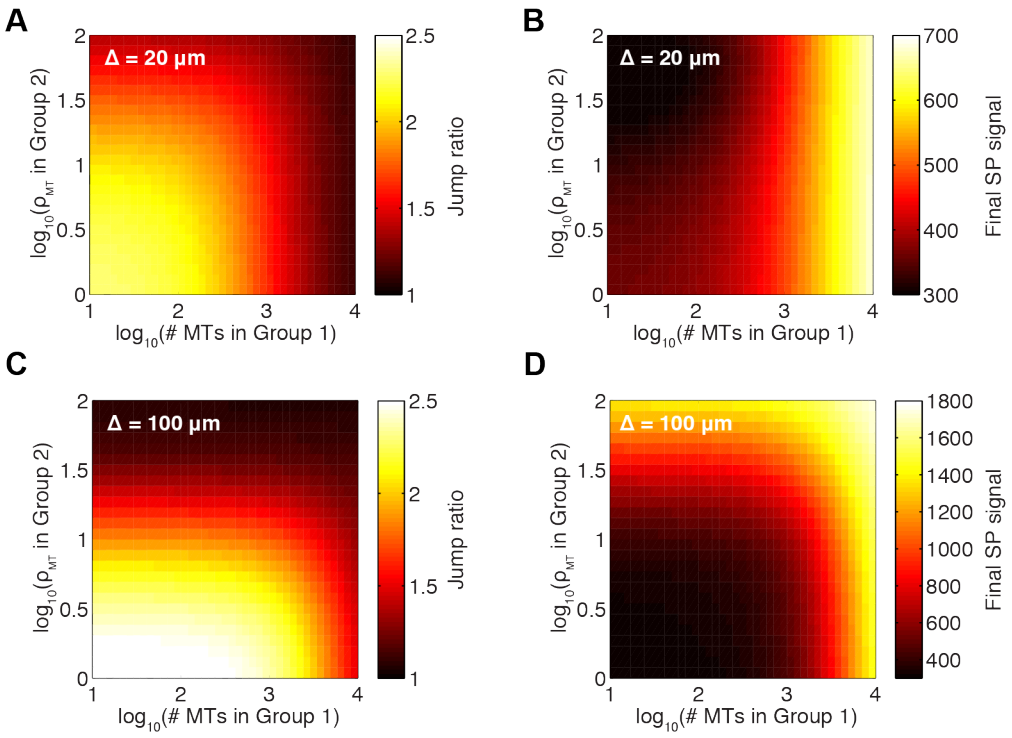

Figure S3: **Dependence of jump ratio and spindle pole signal on microtubule density.**
(**A**) and (**B**) $\Delta = 20\mu m$, $L = W = 10\mu m$, $\delta = 1\mu m$.
(**C**) and (**D**) $\Delta = 100\mu m$, $L = W = 50\mu m$, $\delta = 5\mu m$.
#MTs in Group 1 refers to the number of microtubules associated with one half of the spindle.

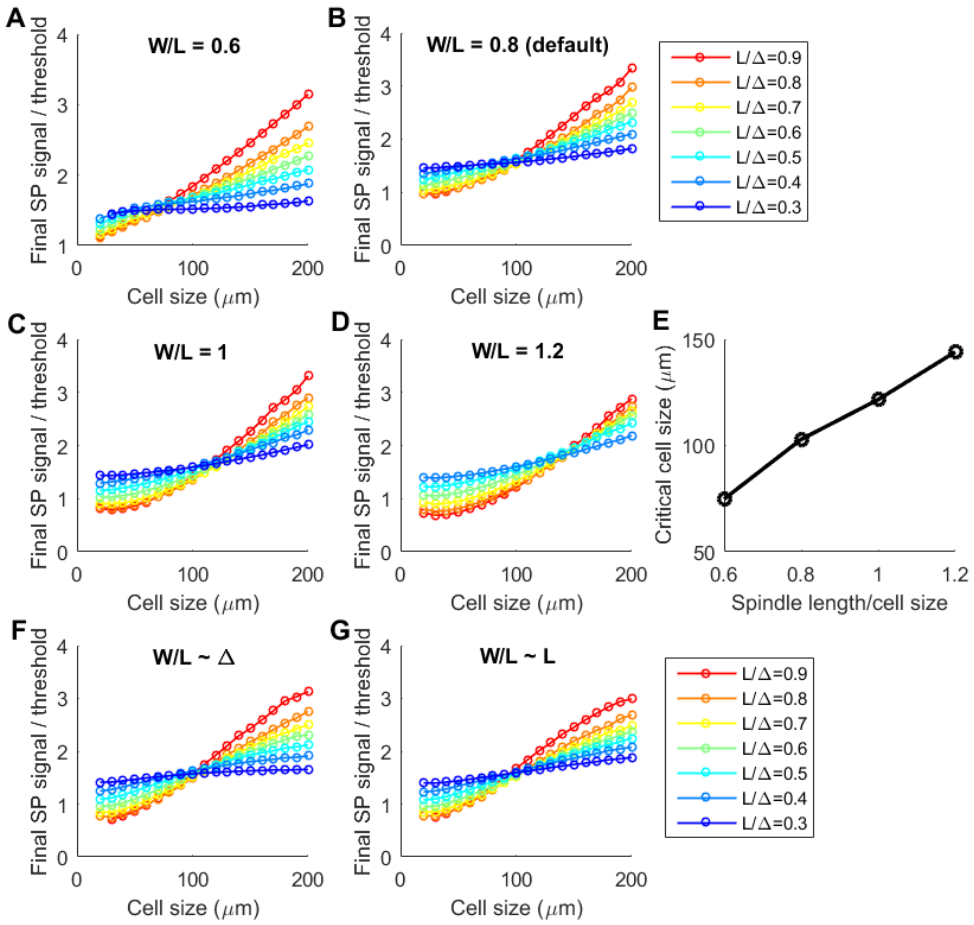

Figure S4: **Transition of relationship between spindle size and spindle pole signal exists for different aspect ratios in spindle.** (**A-D**) Final spindle pole signal as function of cell size and spindle size-cell size ratio at the fixed aspect ratios (W/L = spindle width/spindle length). (B) is identical to Figure 4B. (**E**) Critical cell sizes (where curves intersect) summarized from (A-D). (**F**) Final spindle pole signal as function of cell size and spindle size-cell size ratio when the aspect ratio depends on the cell size as $W/L = 1/(0.8+0.004\times\Delta)$. (**G**) Final spindle pole signal as function of cell size and spindle size-cell size ratio when the aspect ratio depends on the spindle size as $W/L = 1/(0.8+0.006\times L)$. The dependence of aspect ratio on spindle size is motivated by the observation in (1).

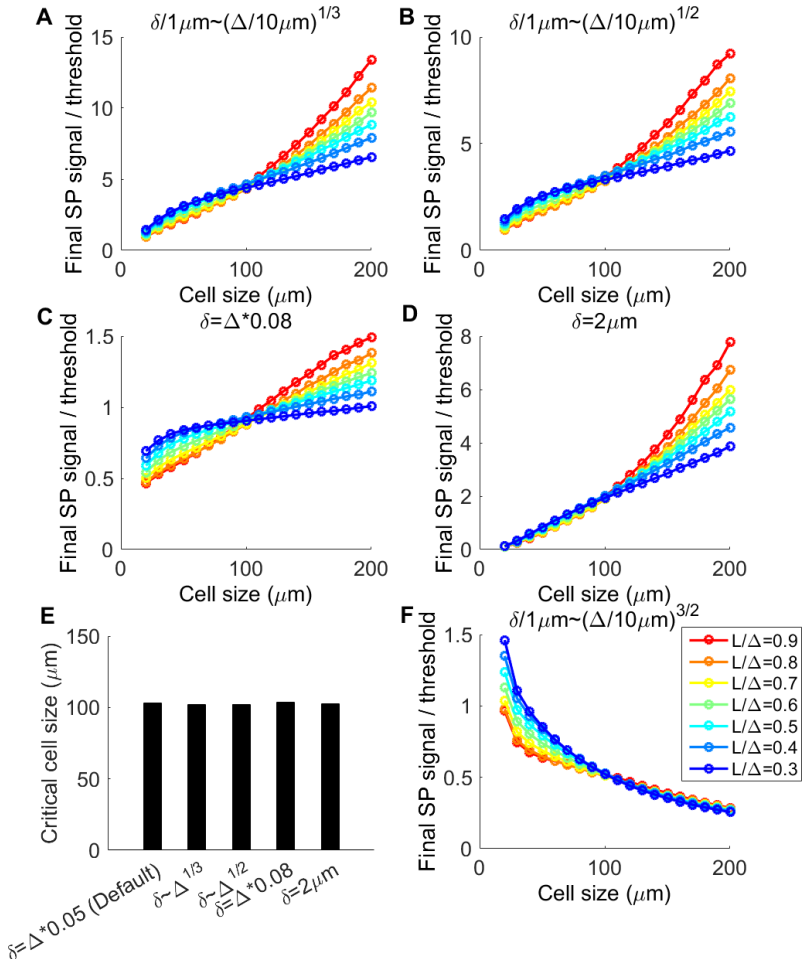

Figure S5: **Transition of relationship between spindle size and spindle pole signal exists for different spindle pole size-cell size relationships.** (**A-D**) Final spindle pole signal as function of cell size and spindle size-cell size ratio at various spindle pole size-cell size relationships as labeled. (**E**) Comparison of the resulting critical cell sizes in (A-D) to the critical cell size found in the default case. (**F**) Final spindle pole signal as function of cell size and spindle size-cell size ratio when the exponent of the spindle pole size-cell size relationship is larger than 1. In this case, the dependence of final spindle pole signal on the cell size is entirely inverted. But in reality, one would not expect spindle pole size to grow faster than cell size. Therefore, this case is not realistic anyway.

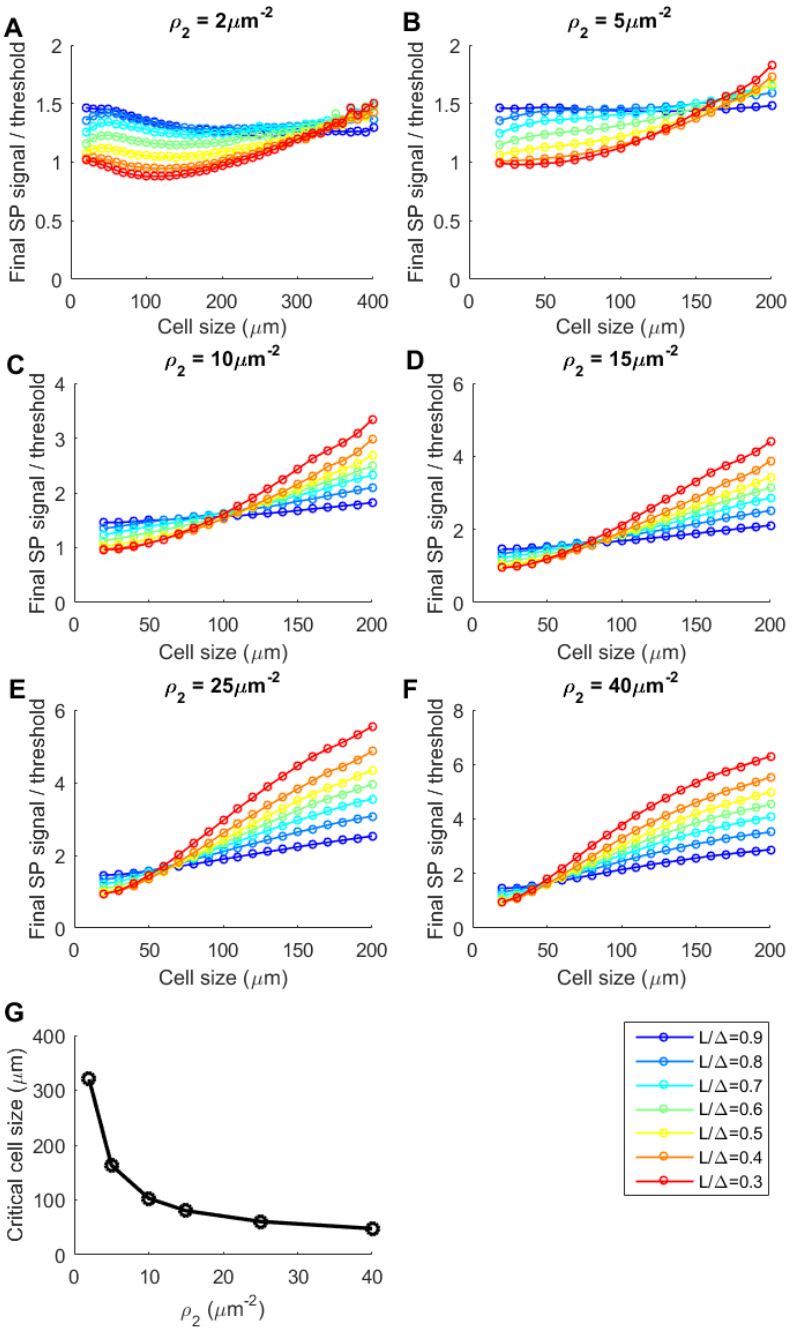

Figure S6: **Transition of relationship between spindle size and spindle pole signal exists for different non-kinetochore microtubule density.** (**A-F**) Final spindle pole signal as function of cell size and spindle size-cell size ratio at various microtubule densities in Group 2. (**G**) Critical cell sizes (where curves intersect) summarized from (A-F).

A

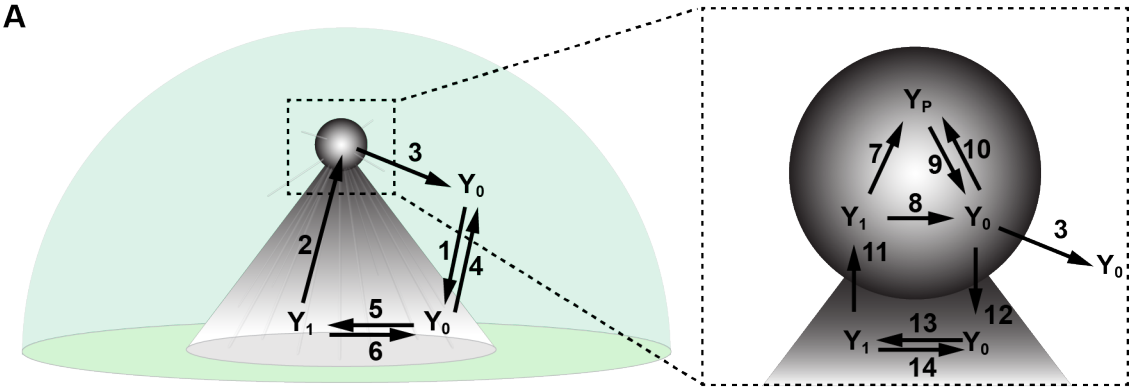

B

Processes	Type	Time scale (τ)	τ for cell size = 20 μm	τ for cell size = 200 μm
#1	diffusion	$\sim \Delta^3 / L / 32D$	~20 s	~2000 s
#2	convection	$\sim L / 2V$	~50 s	~500 s
#3	diffusion	$\sim \delta^2 / 24D$	~0.02 s	~2 s
#4	diffusion	$\sim L^2 / 24D$	~2 s	~200 s
#5	reaction	$\sim 1 / \overline{k}_{\mathrm{onMT}}$ *	~0.1 s	~0.5 s
#6	reaction	$\sim 1 / k_{\mathrm{offMT}}$	~1 s	~1 s
#7	reaction	$\sim 1 / k_{\mathrm{onSP}}$	~0.6 s	~0.6 s
#8	reaction	$\sim 1 / k_{\mathrm{offMT}}^{\mathrm{SP}}$	~0.02 s	~0.02 s
#9	reaction	$\sim 1 / k_{\mathrm{offSP}}$	~30 s	~30 s
#10	reaction	$\sim 1 / k_{\mathrm{onSP}}$	~0.6 s	~0.6 s
#11	convection	$\sim \xi_0 / V$ **	~20 s	~20 s
#12	diffusion	$\sim \delta^2 / 24D$	~0.02 s	~2 s
#13	reaction	$\sim 1 / k_{\mathrm{onMT}}^{\xi}$ ***	~0.01 s	~0.01 s
#14	reaction	$\sim 1 / k_{\mathrm{offMT}}$	~1 s	~1 s

* $\overline{k}_{\mathrm{onMT}}$ represents average microtubule-binding rate of the streaming proteins in the spindle.

** ξ_0 represents the distance from the center of the spindle pole, within which the binding rate with microtubules is much larger than the unbinding rate. This small region around the spindle pole imposes very strong sequestration on the streaming proteins. In this case, ratio between binding and unbinding rates is set to be >100, corresponding to $\xi_0 \sim 2\mu\mathrm{m}$.

*** k_{onMT}^{ξ} represents the average microtubule-binding rate in the region mentioned above. Therefore, it is roughly 100 s^{-1}.

Figure S7: **Transport processes in the spatiotemporal model for SAC.** (**A**) Illustration of the transport processes. The transport processes include convection, diffusion, as well as state conversions (reactions). (**B**) Time scales associated with the processes.

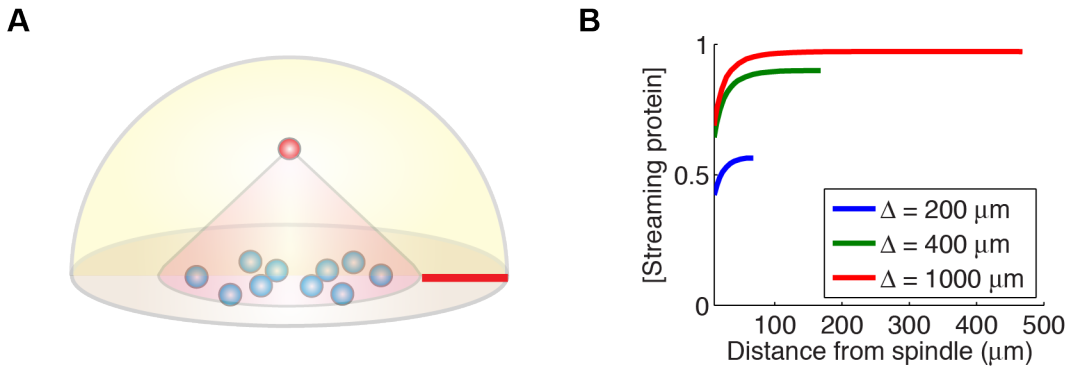

Figure S8: **Gradient of streaming protein outside the spindle.** (**A**) Red line shows the cut line along which the concentration is plotted in (B). (**B**) Gradient of streaming protein concentration fades away from the spindle. When the cell size is really large, the gradients maintain similar level regardless of further increase in cell size. This result explains how the spindle loses sight of the cell boundary for sufficiently large cells. In all simulations, L = 80 μm, W = 64 μm, δ = 10 μm.

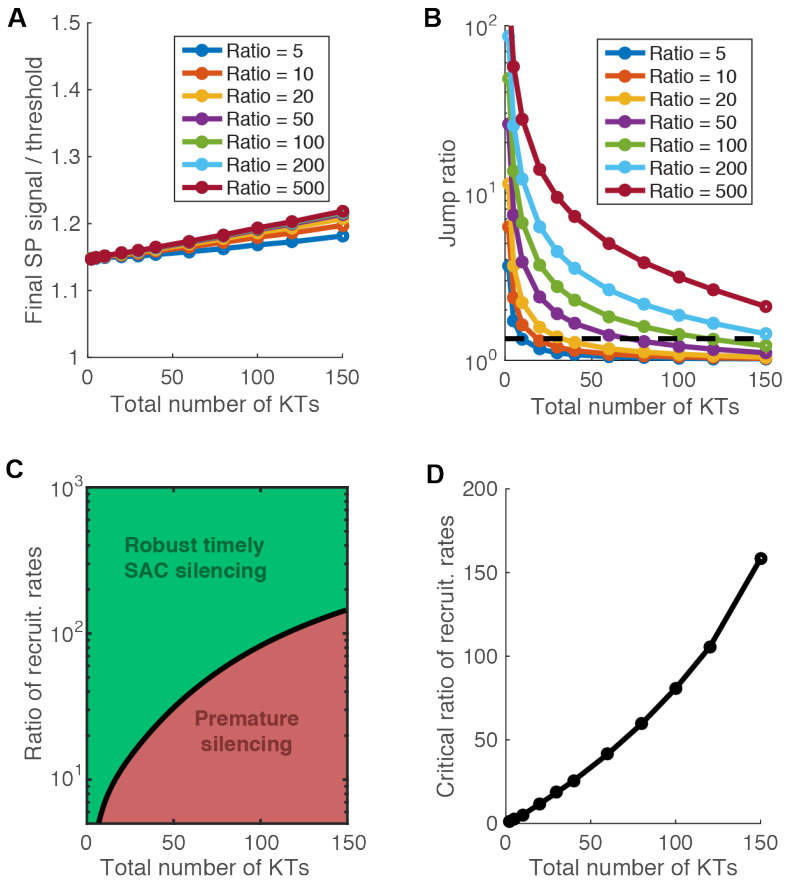

Figure S9: **Increase in recruitment contrast rescues signal robustness diminished by large kinetochore number.** (**A**) Dependence of final steady state spindle pole signal on kinetochore number and contrast ratio between recruitment rates onto unattached versus attached kinetochores. (**B**) Dependence of jump ratio of spindle pole signal on kinetochore number and contrast ratio between recruitment rates onto unattached versus attached kinetochores. Black dashed line: minimum jump ratio 1.35 for robust SAC silencing (see main text for why it is 1.35). (**C**) Phase diagram of mitotic fate based on kinetochore number and contrast ratio between recruitment rates onto unattached versus attached kinetochores. (**D**) Minimum contrast ratio between recruitment rates required to achieve 1.35 jump ratio for different number of kinetochores.

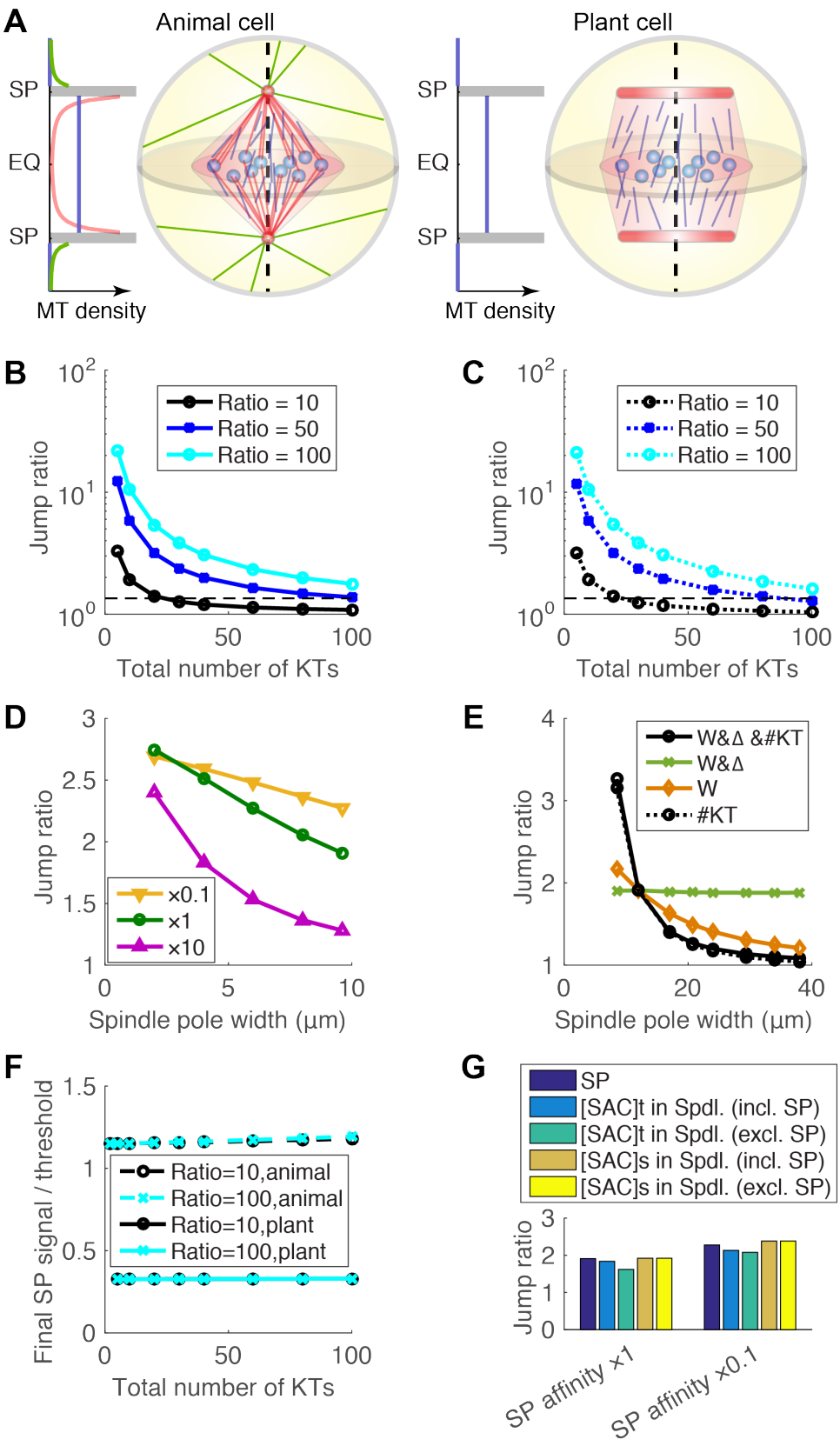
A
Animal cell
Plant cell
SP
EQ
SP
MT density
SP
EQ
SP
MT density
B
Jump ratio
Ratio = 10
Ratio = 50
Ratio = 100
Total number of KTs
C
Jump ratio
Ratio = 10
Ratio = 50
Ratio = 100
Total number of KTs
D
Jump ratio
×0.1
×1
×10
Spindle pole width (μm)
E
Jump ratio
W&Δ &#KT
W&Δ
W
#KT
Spindle pole width (μm)
F
Final SP signal / threshold
Ratio=10,animal
Ratio=100,animal
Ratio=10,plant
Ratio=100,plant
Total number of KTs
G
SP
[SAC]t in Spdl. (incl. SP)
[SAC]t in Spdl. (excl. SP)
[SAC]s in Spdl. (incl. SP)
[SAC]s in Spdl. (excl. SP)
Jump ratio
SP affinity ×1
SP affinity ×0.1

Figure S10: **Possible effect of polyploidy predicted for plant cell mitosis.** (**A**) Comparison of model setup for animal cell vs. plant cell. Red: spindle microtubules in Group 1 characterized by N_1. Blue: spindle microtubules in Group 2 characterized by ρ_2. Green: astral microtubules outside spindle. Specifically, the plant cell has wide spindle poles and loses the microtubules in Group 1 and astral microtubules. (**B**) Jump ratio decreases with ploidy. The volumes of the cell, spindle and spindle pole are proportional to the number of kinetochores by fixed ratios. Different lines show results of different contrast ratios between recruitment of SAC components at unattached versus attached kinetochores. (**C**) Jump ratio decreases with ploidy. The sizes of cell, spindle and spindle pole are kept invariant. Different lines show results of different contrast ratios between recruitment of SAC components at unattached versus attached kinetochores. (**D**) Jump ratio decreases with spindle pole size. Different lines show results with different binding affinities of SAC components at the spindle pole (relative to the default parameter, k_{onSP}, cf. Supplementary Table 1). The decrease is particularly insignificant with low binding affinity at the spindle pole. This is because large spindle pole with high binding affinity causes significant absolute amount of SAC proteins to be sequestered at the spindle pole, thus competing with the diversion effect by the unattached kinetochore. The spindle pole-mediated competition diminishes with either weaker binding affinity or smaller spindle pole. (**E**) Jump ratio depends on ploidy much more than the associated sizing effects. Different lines show results with different combinations of parameters varied. Black solid line: results with volumes of the cell, spindle and spindle pole changing proportional to the number of kinetochores; exactly the same as black solid line in (B). Green solid line: results with constant number of kinetochores, while volumes of the cell, spindle and spindle pole following those in the black solid line. Gold solid line: results with constant number of kinetochores and constant cell size, while volumes of the spindle and spindle pole following those in the black solid line. Black dotted line: results with changing number of kinetochores, yet constant spindle and cell sizing; exactly the same as black dotted line in (C). (**F**) Wider spindle pole reduces concentration of SAC proteins at the spindle pole, potentially below sufficient for triggering SAC silencing. The contrast in recruitment rates does not affect results; so the black solid line overlaps with the cyan solid line and black dashed line overlaps with the cyan dashed line. (**G**) Jump ratio holds up for average SAC concentration in the spindle. The results are nearly same whether the total concentration or the concentration of streaming state SAC components is counted. Results for default spindle pole binding affinity, k_{onSP}, and $k_{\mathrm{onSP}}/10$ are shown.

Supplementary Tables

Supplementary Table 1: **Parameters for transport mechanism in bipolar spindle.**

Parameter	Meaning	Value	Source/Reason
D_{Dyn}	Cytoplasmic diffusion coefficient of microtubule-unbound streaming proteins	2 $\mu m^2\ s^{-1}$	~ Diffusion coefficient of dynein due to huge size of dynein; inferred from diffusion coefficient of APC/C (2).
D_{MT}	Diffusion coefficient of microtubule-bound streaming proteins along microtubule	0.01 $\mu m^2\ s^{-1}$	(3, 4)
D_{Y}	Diffusion coefficient of diffusive proteins	2 $\mu m^2\ s^{-1}$	~ Diffusion coefficient of APC/C (2). No significant difference in model results between spindle pole accumulation of APC/C (D_A = 2 $\mu m^2\ s^{-1}$) and SAC protein (D_M = 20 $\mu m^2\ s^{-1}$) (5).
D_{P}	Diffusion coefficient of spindle pole-bound proteins	2 $\mu m^2\ s^{-1}$	Sufficiently diffusive to homogenize concentration in spindle pole.
D_{K}	Diffusion coefficient of kinetochore-bound proteins	2 $\mu m^2\ s^{-1}$	Sufficiently diffusive to homogenize concentration in kinetochore.
N_1	Number of microtubules associated with each spindle pole in Group 1 (fixed number upon changes of spindle size)	800	(5, 6).
N_{ast}	Number of astral microtubules associated with each spindle pole	800	(5, 6).
ρ_2	Density of microtubules in spindle in Group 2 (fixed density upon changes of spindle size)	10 μm^{-2}	Tubulin concentration inside spindle in Xenopus extract ~ 60 µM (7) ~ 23 μm^{-2}.
V	Processive velocity of microtubule-bound streaming proteins along microtubule	0.1 $\mu m\ s^{-1}$	0.06~0.3 $\mu m\ s^{-1}$ (8, 9).
k_{offMT}	Dissociation rate of streaming proteins from microtubule	1 s^{-1}	*In vitro* unbinding rate 0.05 ~ 1 s^{-1} (10, 11).

k_{onMT}	Association rate of streaming proteins to microtubule	0.17 μm^2 s^{-1} (×microtubule density)	(5, 6).
$k_{\text{offMT}}^{\text{SP}}$	Dissociation rate of streaming proteins from microtubule in spindle pole	40 s^{-1}	Immediate dissociation from the microtubule once entering the spindle pole (see Appendix A).
$k_{\text{onMT}}^{\text{SP}}$	Association rate of streaming proteins to microtubule in spindle pole	0	Immediate dissociation from the microtubule once entering the spindle pole (see Appendix A).
k_{offKT}	Turnover rate from unattached kinetochore	0.2 s^{-1}	1∼60 s turnover time of SAC proteins at the unattached kinetochore (8, 12-14).
$Y_{\text{K}}^{\text{max}}$	Saturating concentration on unattached kinetochore	100 (relative to bulk concentration)	Single unattached kinetochore sequesters ∼0.05% of total cytoplasmic amount of SAC components (12); ratio between kinetochore volume and cell volume ∼ 10^{-5} → kinetochore concentration ∼ 10^2 bulk average in cell.
k_{onKTu}	Recruitment rate onto unattached kinetochore	200 s^{-1}	(5); to saturate the unattached kinetochore.
k_{onKTt}	Recruitment rate onto attached kinetochore	2 s^{-1}	(5); << k_{onKTu} due to attachment/tension induced change in kinase effect.
k_{DoffKT}	Release rate of poleward streaming proteins from attached kinetochore	20 s^{-1}	(5); $k_{\text{DoffKT}} > k_{\text{onKTt}}$ such that the attached kinetochores do not accumulate protein.
k_{offSP}	Unbinding rate of proteins from spindle pole	0.0333 s^{-1}	∼ 30s turnover time at spindle pole (15).
k_{onSP}	Binding rate of proteins to spindle pole	1.8 s^{-1}	(5)
U_{ext}	Sequestration potential around the spindle boundary	2 k_BT, 1 μm width	

Supplementary References

1. Young, S., S. Besson, and J. P. Welburn. 2014. Length-dependent anisotropic scaling of spindle shape. Biology open 3:1217-1223.
2. Wang, Z. F., J. V. Shah, M. W. Berns, and D. W. Cleveland. 2006. In vivo quantitative studies of dynamic intracellular processes using fluorescence correlation spectroscopy. Biophysical journal 91:343-351.
3. Wang, Z. H., and M. P. Sheetz. 1999. One-dimensional diffusion on microtubules of particles coated with cytoplasmic dynein an immunoglobulins. Cell Structure and Function 24:373-383.
4. Ross, J. L., K. Wallace, H. Shuman, Y. E. Goldman, and E. L. F. Holzbaur. 2006. Processive bidirectional motion of dynein-dynactin complexes in vitro. Nature cell biology 8:562-570.
5. Chen, J., and J. Liu. 2014. Spatial-temporal model for silencing of the mitotic spindle assembly checkpoint. Nature communications 5:4795.
6. Chen, J., J. Lippincott-Schwartz, and J. Liu. 2012. Intracellular spatial localization regulated by the microtubule network. PloS one 7:e34919.
7. Needleman, D. J., A. Groen, R. Ohi, T. Maresca, L. Mirny, and T. Mitchison. 2010. Fast Microtubule Dynamics in Meiotic Spindles Measured by Single Molecule Imaging: Evidence That the Spindle Environment Does Not Stabilize Microtubules. Molecular Biology of the Cell 21:323-333.
8. Famulski, J. K., L. J. Vos, J. B. Rattner, and G. K. Chan. 2011. Dynein/Dynactin-mediated transport of kinetochore components off kinetochores and onto spindle poles induced by nordihydroguaiaretic acid. PloS one 6:e16494.
9. Heald, R., R. Tournebize, A. Habermann, E. Karsenti, and A. Hyman. 1997. Spindle assembly in Xenopus egg extracts: respective roles of centrosomes and microtubule self-organization. The Journal of cell biology 138:615-628.
10. King, S. J., and T. A. Schroer. 2000. Dynactin increases the processivity of the cytoplasmic dynein motor. Nature cell biology 2:20-24.
11. Reck-Peterson, S. L., A. Yildiz, A. P. Carter, A. Gennerich, N. Zhang, and R. D. Vale. 2006. Single-molecule analysis of dynein processivity and stepping behavior. Cell 126:335-348.
12. Howell, B. J., B. Moree, E. M. Farrar, S. Stewart, G. W. Fang, and E. D. Salmon. 2004. Spindle checkpoint protein dynamics at kinetochores in living cells. Current Biology 14:953-964.
13. Shah, J. V., E. Botvinick, Z. Bonday, F. Furnari, M. Berns, and D. W. Cleveland. 2004. Dynamics of centromere and kinetochore proteins: Implications for checkpoint signaling and silencing. Current Biology 14:942-952.
14. Basto, R., F. Scaerou, S. Mische, E. Wojcik, C. Lefebvre, R. Gomes, T. Hays, and R. Karess. 2004. In vivo dynamics of the rough deal checkpoint protein during Drosophila mitosis. Current Biology 14:56-61.
15. Famulski, J. K., L. Vos, X. Sun, and G. Chan. 2008. Stable hZW10 kinetochore residency, mediated by hZwint-1 interaction, is essential for the mitotic checkpoint. The Journal of cell biology 180:507-520.